X-ray Crystal Structures of D100E Trichodiene Synthase and Its Pyrophosphate Complex Reveal the Basis for Terpene Product Diversity[†,‡]

Michael J. Rynkiewicz,[§] David E. Cane,[||] and David W. Christianson*[,§]

Department of Chemistry, University of Pennsylvania, Philadelphia, Pennsylvania 19104-6323, and Department of Chemistry, Brown University, Providence, Rhode Island 02912

Received October 23, 2001; Revised Manuscript Received December 6, 2001

ABSTRACT: The 2.4 Å resolution X-ray crystal structure of D100E trichodiene synthase and the 2.6 Å resolution structure of its complex with inorganic pyrophosphate are reported. The D100E amino acid substitution in the so-called "aspartate-rich" motif does not result in large changes to the overall structure of the enzyme. In the pyrophosphate complex, however, pyrophosphate coordinates two Mg^{2+} ions at the mouth of the active site without causing large changes in the structure of the enzyme. This contrasts with pyrophosphate binding in the wild-type enzyme, where pyrophosphate coordinates three Mg^{2+} ions and triggers a significant conformational change that closes the mouth of the active site and optimizes packing density in the enzyme−substrate complex. The attenuation of active site closure in D100E trichodiene synthase compromises enzyme−substrate packing density and confers additional spatial and conformational degrees of freedom on the substrate and carbocation intermediates, which in turn results in the formation of five alternate sesquiterpene products in addition to trichodiene. By extension, then, the diversity of terpene cyclases in biology may have evolved in part by amino acid substitutions that fine-tune structural changes dependent on metal−diphosphate complexation that govern the formation of the active site template and enzyme−substrate packing density.

Sesquiterpenes are hydrocarbon compounds that derive from a single precursor molecule, farnesyl diphosphate, in a wide variety of organisms. Sesquiterpene cyclases (also known as sesquiterpene synthases) are metal-dependent enzymes that convert farnesyl diphosphate into over 300 different cyclic sesquiterpenes with widely varying structures and stereochemistries (*1*−*5*). Four X-ray crystal structures of sesquiterpene cyclases have been reported to date: pentalenene synthase from *Streptomyces* UC5319 (*6*), 5-*epi*-aristolochene synthase from *Nicotiana tabacum* (*7*), aristolochene synthase from *Penicillium roqueforti* (*8*), and, most recently, trichodiene synthase from *Fusarium sporotrichioides* (*9*). The structures of these cyclases are remarkably similar despite a lack of significant amino acid sequence identity. Such structural similarity suggests evolution from a common ancestral enzyme that, subject to different evolutionary pressures in a variety of life forms, underwent mutation to yield diverse active site topologies.

The role of metal ions in sesquiterpene biosynthesis is well studied. All sesquiterpene cyclases contain the consensus "aspartate-rich motif", DDXX(D,E), and X-ray crystal structures show that this motif binds Mg^{2+} in trichodiene synthase (*9*), 5-*epi*-aristolochene synthase (*7*), and farnesyl diphosphate synthase (*10*) and Sm^{3+} in aristolochene synthase (*8*). This motif appears as D^{100}DSKD in trichodiene synthase, and the D100 carboxylate coordinates two Mg^{2+} ions with *syn*,*syn*-bidentate geometry in the complex with inorganic pyrophosphate and, presumably, with farnesyl diphosphate as well (*9*). Importantly, the residues in the aspartate-rich motif also mediate a diphosphate-induced conformational change that closes the active site to solvent (*9*). Accordingly, it is not surprising that even the conservative D100E[1] amino acid substitution results in a 22-fold loss of activity as measured by k_{cat}/K_M (*11*). Surprisingly, however, D100E trichodiene synthase also produces five sesquiterpene products in addition to trichodiene, including the newly characterized terpene, isochamigrene (Figure 1) (*12*). Thus, this mutant represents in effect an in vitro evolutionary step toward the biosynthesis of novel sesquiterpene products.

Here, the X-ray crystal structure of D100E trichodiene synthase is reported in both the unliganded state (2.4 Å resolution) and in complex with the reaction product pyrophosphate (2.6 Å resolution). Comparison of these structures with the corresponding structures of the wild-type enzyme reveals the structural basis for the evolution of product specificity. In particular, a significant diphosphate-induced conformational change is severely attenuated in the mutant, thus opening alternate reaction pathways to the substrate.

MATERIALS AND METHODS

The D100E mutant of trichodiene synthase from *F. sporotrichioides* was previously prepared and overexpressed

[†] This work was supported by National Institutes of Health Grant GM56838 (to D.W.C.) and Merit Award GM30301 (to D.E.C.).

[‡] Atomic coordinates of D100E trichodiene synthase and its complex with diphosphate have been deposited in the Protein Data Bank with accession codes 1KIY and 1KIZ, respectively.

* To whom correspondence should be addressed at the Department of Chemistry, University of Pennsylvania, 231 South 34th St., Philadelphia, PA 19104-6323 [215 898-5714 (office); 215 573-2201 (fax); chris@rock.chem.upenn.edu (e-mail)].

[§] University of Pennsylvania.

[||] Brown University.

[1] Abbreviations: D100E, aspartate-100 → glutamate; rms, root mean square.

10.1021/bi011960g CCC: $22.00
Published on Web 01/17/2002

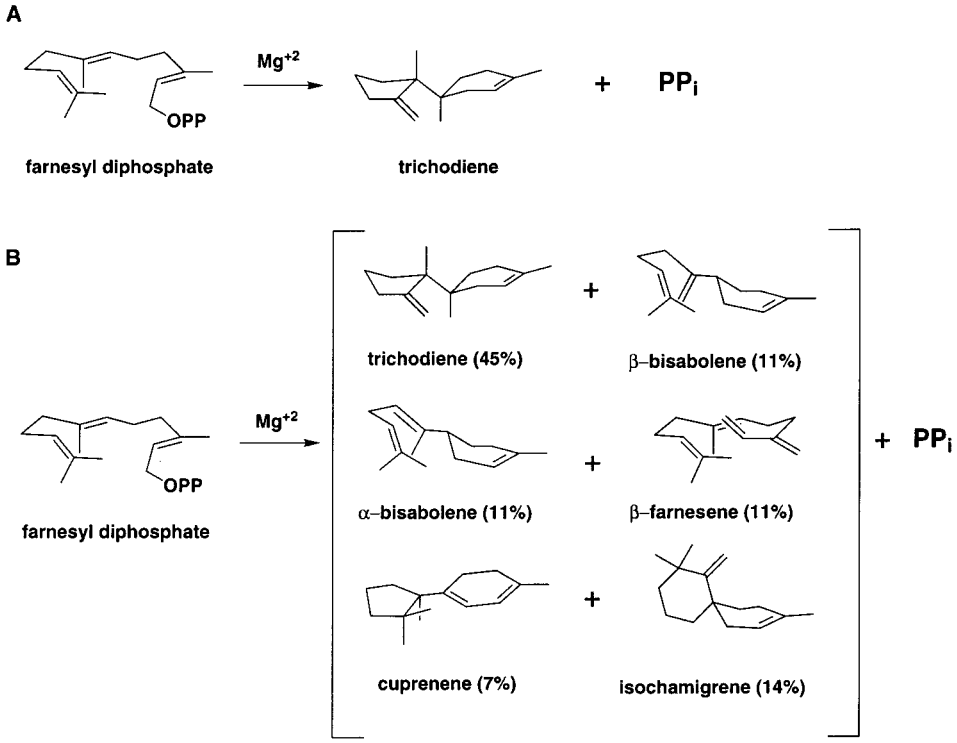

FIGURE 1: (A) Cyclization reaction catalyzed by trichodiene synthase. (B) Sesquiterpene products generated by D100E trichodiene synthase (OPP = diphosphate; PP_i = inorganic pyrophosphate). Relative yields of each product are in parentheses.

in *Escherichia coli* (*13*). The mutant enzyme was purified and crystallized in the same manner as described for the wild-type enzyme (*9*), and crystals were soaked with pyrophosphate using the same protocol as described for the wild-type enzyme−pyrophosphate complex (*9*). The mutant crystallizes isomorphously with the wild-type enzyme (space group $P3_121$, $a = b = 122.7$ Å, $c = 151.5$ Å) with two molecules in the asymmetric unit, chain A and chain B. Diffraction data for both unliganded and pyrophosphate-liganded enzyme crystals were collected at Argonne National Laboratories SBC-CAT (beamline 19-ID). Data were indexed and merged using the program HKL2000 (*14*). The structures were solved using difference Fourier techniques using the wild-type−pyrophosphate complex (consisting of two chains with 354 residues each less the pyrophosphate, Mg^{2+} ions, and solvent molecules) as a starting model. The programs CNS (*15*) and O (*16*) were used in refinement and rebuilding, respectively. Noncrystallographic symmetry restraints were applied throughout the refinement. The root mean square deviations between monomers A and B are 0.11 and 0.27 Å for 354 C_α atoms for the final structures of unliganded D100E trichodiene synthase and its pyrophosphate complex, respectively. Electron density for the pyrophosphate ligand was observed only in the active site of chain B, possibly due to a crystal contact that partially occludes the active site of chain A. Data collection and refinement statistics are reported in Table 1.

For modeling of enzyme−substrate and enzyme−intermediate complexes, the program MacroModel (*17*) was used to generate energy-minimized structures of farnesyl diphosphate, reaction intermediates, and products with explicit hydrogens included subject to conformational constraints consistent with specific bond-making and bond-breaking steps in trichodiene formation (*3*, *18*−*20*). These models were then manually docked into the enzyme active site using O, and bad contacts between enzyme and model were alleviated by 20 cycles of rigid body minimization followed by 200 cycles of conjugate gradient minimization using CNS. During refinement, pyrophosphate and Mg^{2+} atoms were fixed, with a harmonic restraint of 10 kcal mol^{-1} $Å^{-2}$ applied to the hydrocarbon portion of the substrate, intermediate, or product. Nonbonded interactions in the crystal lattice were included in the minimization, but no other constraints were applied to the protein atoms. Explicit hydrogen atoms were included on the enzyme but not on the substrate, intermediate, or products. Energy minimizations calculated with and without explicit hydrogen atoms on a test set of intermediates yielded identical results.

Calculations of the active site volume were performed using the program VOIDOO (*21*−*23*). The volume reported

Table 1: Data Collection and Refinement Statistics

data set	D100E	diphosphate complex
resolution range (Å)	25−2.4	25−2.6
reflections (measured/unique)	295631/52222	246608/41214
completeness (%) (overall/outer shell)	99.8/100	99.8/100
R_{merge}[a] (overall/outer shell)	0.074/0.366	0.081/0.237
protein atoms (no.)	5884	5884
solvent atoms (no.)	382	240
ligand atoms (no.)	0	11
reflections used in refinement (work/free)	44195/3854	37680/3111
R/R_{free}[b]	0.215/0.248	0.223/0.256
rms deviations		
bonds (Å)	0.007	0.007
angles (deg)	1.1	1.1
proper dihedrals (deg)	19.1	19.0
improper dihedrals (deg)	0.8	0.8

[a] $R_{merge} = \sum|I_j - \langle I\rangle_j|/\sum I_j$, where I_j is the observed intensity for reflection j and $\langle I\rangle_j$ is the average intensity calculated for reflection j from replicate data. [b] $R = \sum||F_o| - |F_c||/\sum|F_o|$, where R and R_{free} are calculated by using the working and test reflection sets, respectively.

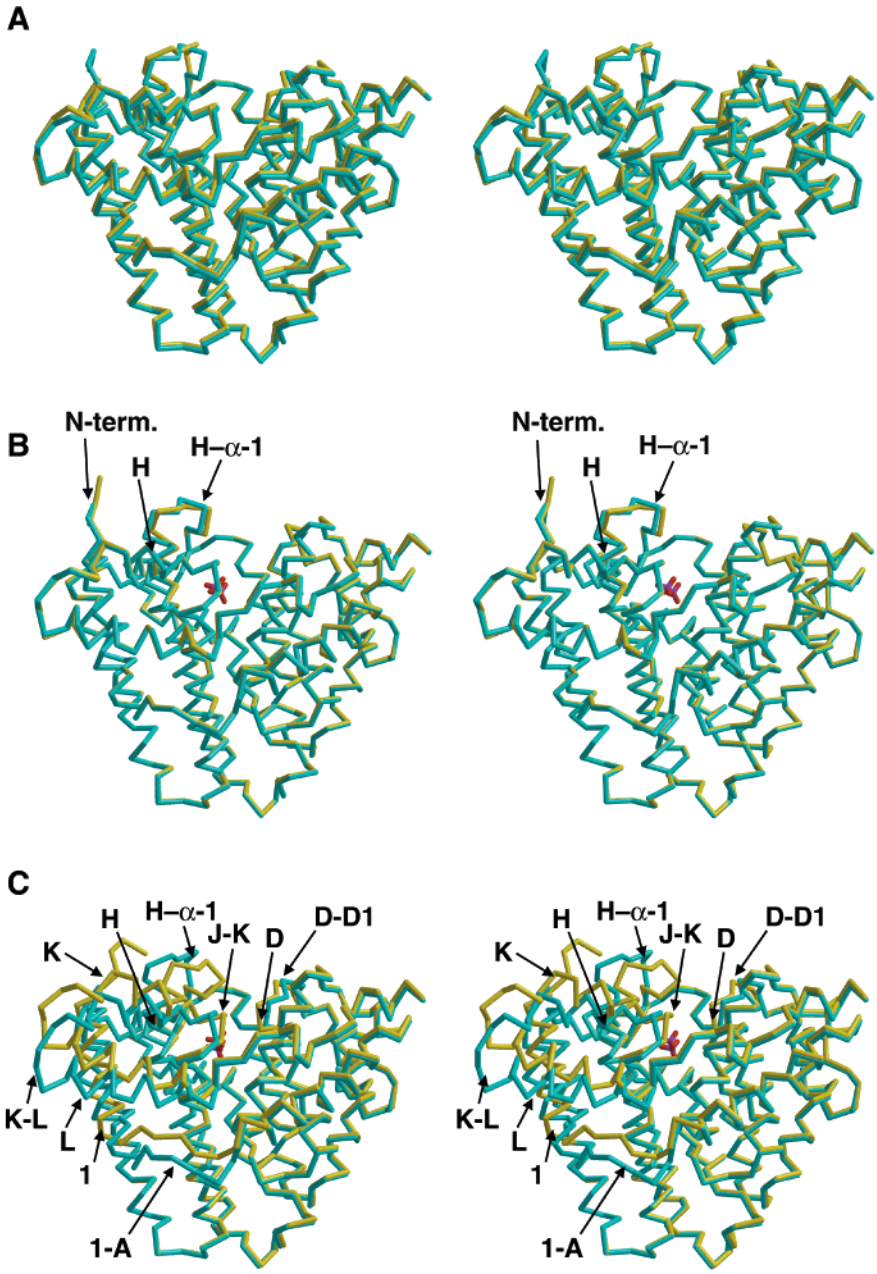

FIGURE 2: The B monomers in trichodiene synthase crystals. (A) Superposition of the C_α traces of wild-type (yellow) and D100E (cyan) trichodiene synthases. (B) Superposition of the C_α traces of D100E trichodiene synthase, unliganded (cyan) and complexed with pyrophosphate (yellow). The residues that undergo conformational change are indicated as follows: N-terminus = 1−5, H = 229−233, and H−α-1 = 233−241. (C) Superposition of the C_α traces of wild-type trichodiene synthase, unliganded (cyan) and complexed with pyrophosphate (yellow). The residues that undergo conformational change are indicated as follows: 1 = 6−19, 1−A = 19−29, D = 99−102, D−D1 = 103−105, D2 = 113−119, H = 229−233, H−α-1 = 233−241, J−K = 300−307, K = 307−311, K−L = 312−319, and L = 320−336. Pyrophosphate-induced conformational changes in the wild-type enzyme are much more pronounced than those observed in the D100E mutant.

is the volume occupied by a probe sphere of 1.4 Å radius in the active site cavity. Each volume calculation was repeated 10 times with randomly oriented models and averaged to remove orientational errors, as instructed by the program authors (*22*). Volume calculations on substrates and intermediates include explicit hydrogens and were performed using the program MacroModel (*17*).

RESULTS

The D100E substitution does not significantly perturb the overall structure of trichodiene synthase, and the root mean square (rms) deviation of 349 C_α atoms between the wild-type and mutant structures is 0.56 Å (Figure 2A). Electron density maps of unliganded and pyrophosphate-liganded D100E trichodiene synthase clearly reveal the substitution of aspartate by the longer side chain of glutamate at position 100 in the aspartate-rich motif (Figure 3A).

The structure of the D100E trichodiene synthase−pyrophosphate complex is significantly different from that of the wild-type enzyme−pyrophosphate complex. In the mutant, the liganded structure superposes onto the unliganded structure with an rms deviation of 0.44 Å for 354 C_α atoms (Figure 2B). This contrasts with the much greater structural differences observed in the wild-type enzyme, for which the

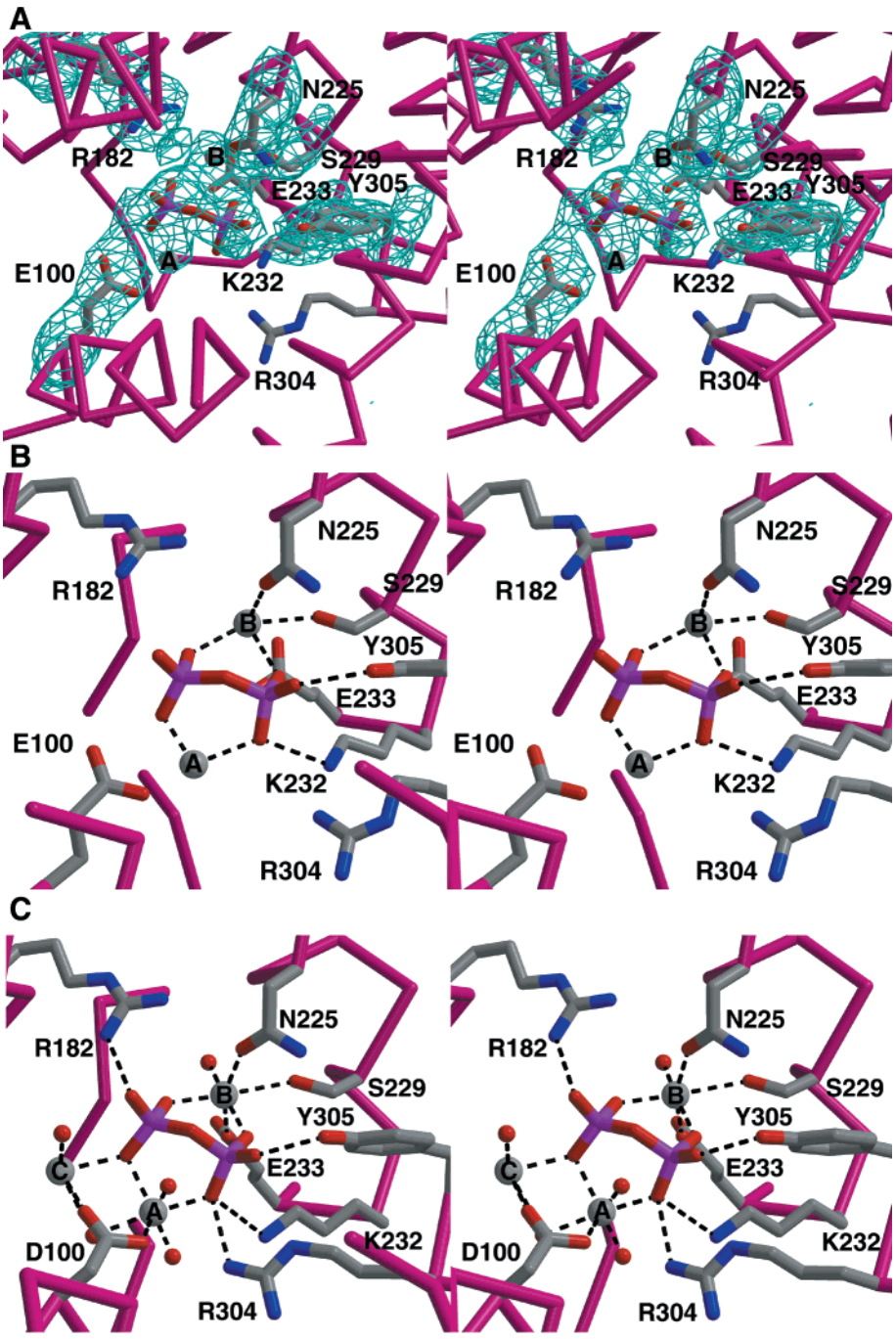

FIGURE 3: (A) Simulated annealing omit map of the active site of the D100E trichodiene synthase−pyrophosphate complex (contoured at 3σ); pyrophosphate, Mg^{2+} ions, and residues within 3.5 Å of pyrophosphate and Mg^{2+} were omitted from the structure factor calculation. (B) Hydrogen-bonding interactions in the pyrophosphate complex of D100E. Note the differences in interactions with the wild-type−pyrophosphate complex shown with the same view (C).

liganded structure superposes onto the unliganded structure with an rms deviation of 1.42 Å for 349 C_α atoms (Figure 2C). In both wild-type and mutant enzymes, pyrophosphate caps the active site cleft and sequesters it from solvent. That the alternate products formed in the mutant reaction do not arise from premature nucleophilic quenching by water is consistent with this observation. However, the active site cavity thus formed has a greater volume (364 ± 4 Å^3) in the mutant than that observed in the wild-type enzyme−pyrophosphate complex (324 ± 5 Å^3). For reference, the volume of the hydrocarbon product of the reaction, trichodiene, is 230 Å^3.

Clearly, the wild-type enzyme exhibits a pyrophosphate-induced conformational change that is severely attenuated in the D100E mutant. In the wild-type enzyme, pyrophosphate binding causes up to 6 Å structural changes in the C_α atoms of helix 1, the 1−A loop, helix D, the D−D1 loop, helix H, the H−α-1 loop, helix J, the J−K loop, helix K, the K−L loop, and helix L (Figure 2C) (*9*). In the D100E mutant, the only structural changes triggered by pyrophosphate binding are in the first five residues of the N-terminus, helix H, and the H−α-1 loop (residues 229−241) (Figure 2B). The helix H−H−α-1 loop region has high average *B* factors in both unliganded and liganded structures (63 and

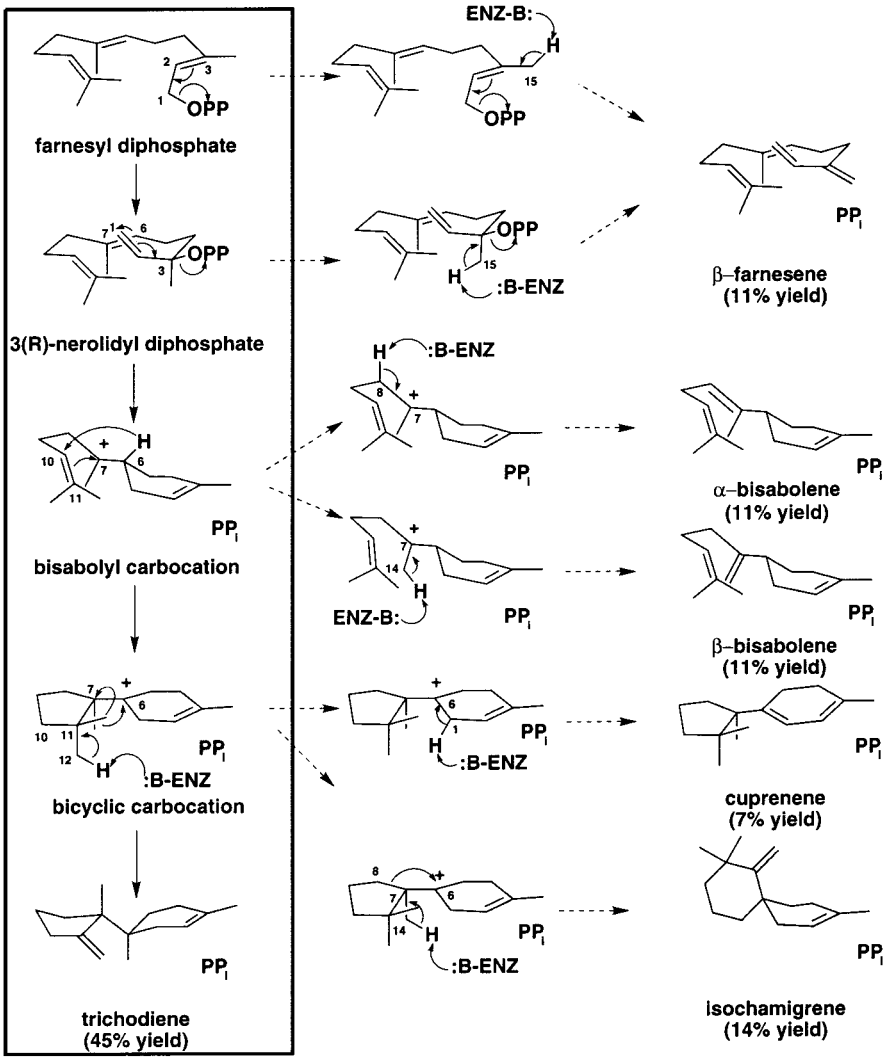

FIGURE 4: Mechanisms of product formation by D100E trichodiene synthase (OPP = diphosphate; PP_i = inorganic pyrophosphate). On the basis of analysis of the crystal structure, possible candidates for the catalytic bases (:B-ENZ) are inorganic pyrophosphate and the side chains of E100, Y295, and/or Y305.

88 Å^2, respectively), so observed differences in this segment may arise from conformational disorder. Additionally, in the wild-type enzyme a new hydrogen bond forms between D101 and R304 upon pyrophosphate binding. In the D100E mutant−pyrophosphate complex, this hydrogen bond is absent: D101 remains hydrogen bonded to R62, as observed in the unliganded wild-type enzyme structure (*9*).

The active site of the mutant complexed with pyrophosphate shows electron density consistent with two Mg^{2+} ions and one molecule of inorganic pyrophosphate (Figure 3A,B). This contrasts with the corresponding structure of the wild-type enzyme−pyrophosphate complex, in which three Mg^{2+} ions are observed (Figure 3C). The average *B* factor of the ligand atoms (85 Å^2) is high compared to the rest of the protein chain (43 Å^2), probably due to low-occupancy ligand binding. Also, in contrast with the wild-type enzyme−pyrophosphate complex, pyrophosphate does not hydrogen bond with R182 and R304 in the D100E mutant. The pyrophosphate position is shifted ~1.3 Å from its position in the wild-type enzyme−pyrophosphate complex.

Interestingly, the Mg^{2+}_A and Mg^{2+}_B sites in the mutant are compromised by the D100E mutation (Mg^{2+}_C is not visible). In the wild-type enzyme−pyrophosphate complex, Mg^{2+}_B is coordinated by the side chains of N225, S229, and E233. The Mg^{2+}_B binding site loses one coordination interaction with the side chain of E233 in the mutant. In the wild-type enzyme−pyrophosphate complex, D100 coordinates Mg^{2+}_A and Mg^{2+}_C with *syn*,*syn*-bidentate geometry. In the mutant, the Mg^{2+}_A−E100 carboxylate separation is increased by 1 Å. Therefore, E100 makes only a long-range electrostatic interaction with Mg^{2+}_A. Weaker binding of Mg^{2+}_A results, and Mg^{2+}_A is accordingly characterized by a weaker electron density peak. The electropositive environment surrounding the diphosphate leaving group of farnesyl diphosphate would thus be weaker in D100E trichodiene synthase than in the wild-type enzyme due to the binding of only two Mg^{2+} ions and the loss of two critical diphosphate−arginine contacts.

DISCUSSION

The mechanism of trichodiene biosynthesis has been extensively studied (Figure 4) (*3*, *18*−*20*). Briefly, ionization of farnesyl diphosphate and recapture of the pyrophosphate ion result in isomerization to (3*R*)-nerolidyl diphosphate, which can undergo rotation about the newly generated C2−C3 bond from a transoid to a cisoid conformation. Reion-

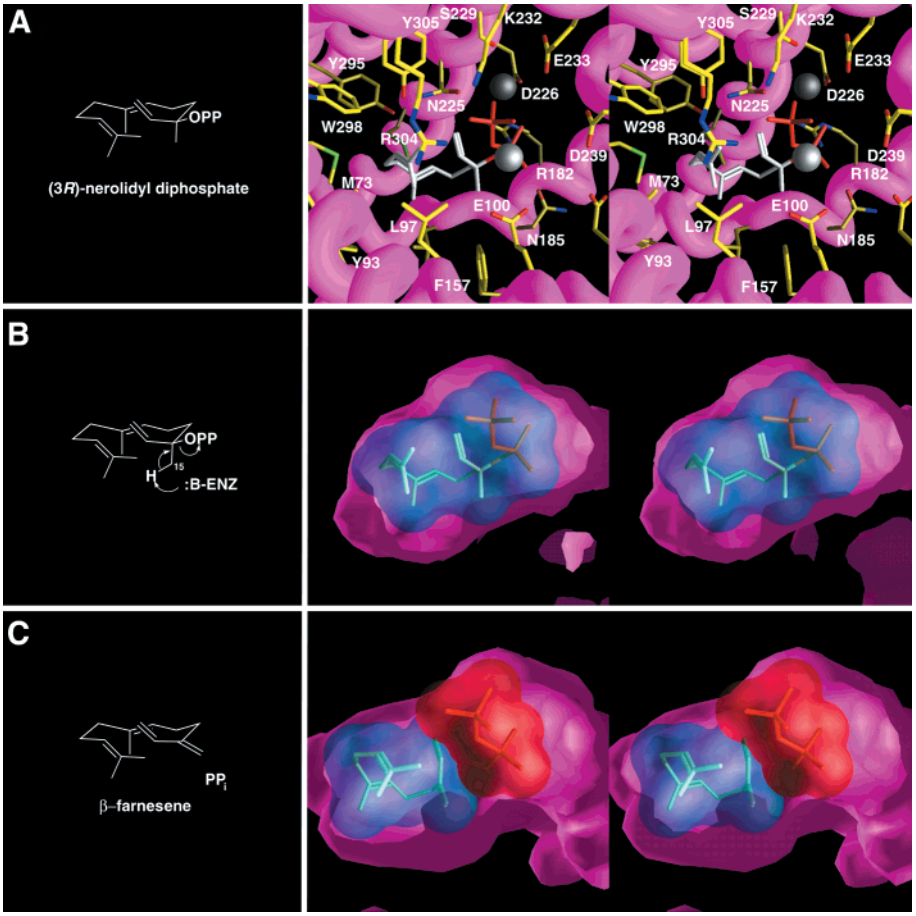

FIGURE 5: β-Farnesene synthesis. (A) Model of (3*R*)-nerolidyl diphosphate in the D100E active site. The Mg^{2+} ions are silver spheres. (B) The molecular surfaces of the protein (magenta) and (3*R*)-nerolidyl diphosphate (cyan) are displayed. (C) Deprotonation of C15, possibly by pyrophosphate, results in the formation of β-farnesene. The molecular surface of the diphosphate leaving group is in red. This figure was prepared with GRASP (*24*).

ization of (3*R*)-nerolidyl diphosphate and electrophilic attack by the C1 carbocation on the C6−C7 π bond yield the bisabolyl carbocation intermediate. The C6 carbocation then attacks the C10−C11 π bond to form the five-membered ring of the first bicyclic intermediate. This species, with a carbocation at C10, subsequently undergoes a 1,4-hydride shift from C6, followed by tandem methyl migrations from C7 to C6 and then from C11 to C7, with final deprotonation at C12 to yield trichodiene.

Structural and enzymological studies of trichodiene synthase have implicated D100 in catalysis (*9*, *11*, *12*). Mutation of this residue to glutamate results in more than a 20-fold decrease in k_{cat}/K_M, resulting from a combined 2.5-fold decrease in k_{cat} and an 8-fold increase in K_M (*11*). The rate-determining step for wild-type trichodiene synthase has been shown by rapid chemical quench and single turnover experiments to be product release, which occurs at a rate 40 times slower than the rate of substrate ionization (*20*). For the observed 2.5-fold net reduction of k_{cat} for the D100E mutant, the slow product off-rate therefore should mask a more profound decrease in the rate of farnesyl diphosphate consumption. Indeed, single turnover experiments on the D101E mutant, which exhibits an 5.5-fold decrease in k_{cat}/K_M resulting from a combined 3.4-fold decrease in k_{cat} and an 1.6-fold increase in K_M (*11*), have shown a nearly 100-fold decrease in the rate of substrate consumption. Most interestingly, these two mutants, as well as the D104E mutant from the same aspartate-rich motif, all showed formation of five aberrant products in addition to the natural trichodiene (*11*, *12*).

Here, we demonstrate for the first time the structural consequences of the D100E substitution: pyrophosphate binding geometry is perturbed such that only two Mg^{2+} ions bind, and the pyrophosphate position in the active site is shifted. This strongly implies that the diphosphate position is likewise perturbed in the enzyme−substrate complex, and this situation likely leads to aberrant product formation. That the active site in the D100E trichodiene synthase−pyrophosphate complex is 12% larger than in the corresponding complex with the wild-type enzyme additionally complicates the cyclization reaction by allowing for multiple substrate binding conformations, which in turn can contribute to aberrant product formation. Modeling studies of the wild-type enzyme implicate the side chain of D100, or the diphosphate molecule itself, as the catalytic base in the final step of the reaction (*9*). Therefore, with the D100E substitution, the position of the catalytic base is potentially altered; moreover, E100 may or may not serve as a catalytic base in alternate cyclization cascades.

The structural basis for aberrant product formation by D100E trichodiene synthase can be rationalized from the structure of the enzyme and the well-studied mechanism of trichodiene synthesis (*15*) (Figure 4). Four of the aberrant products result from premature deprotonation of intermedi-

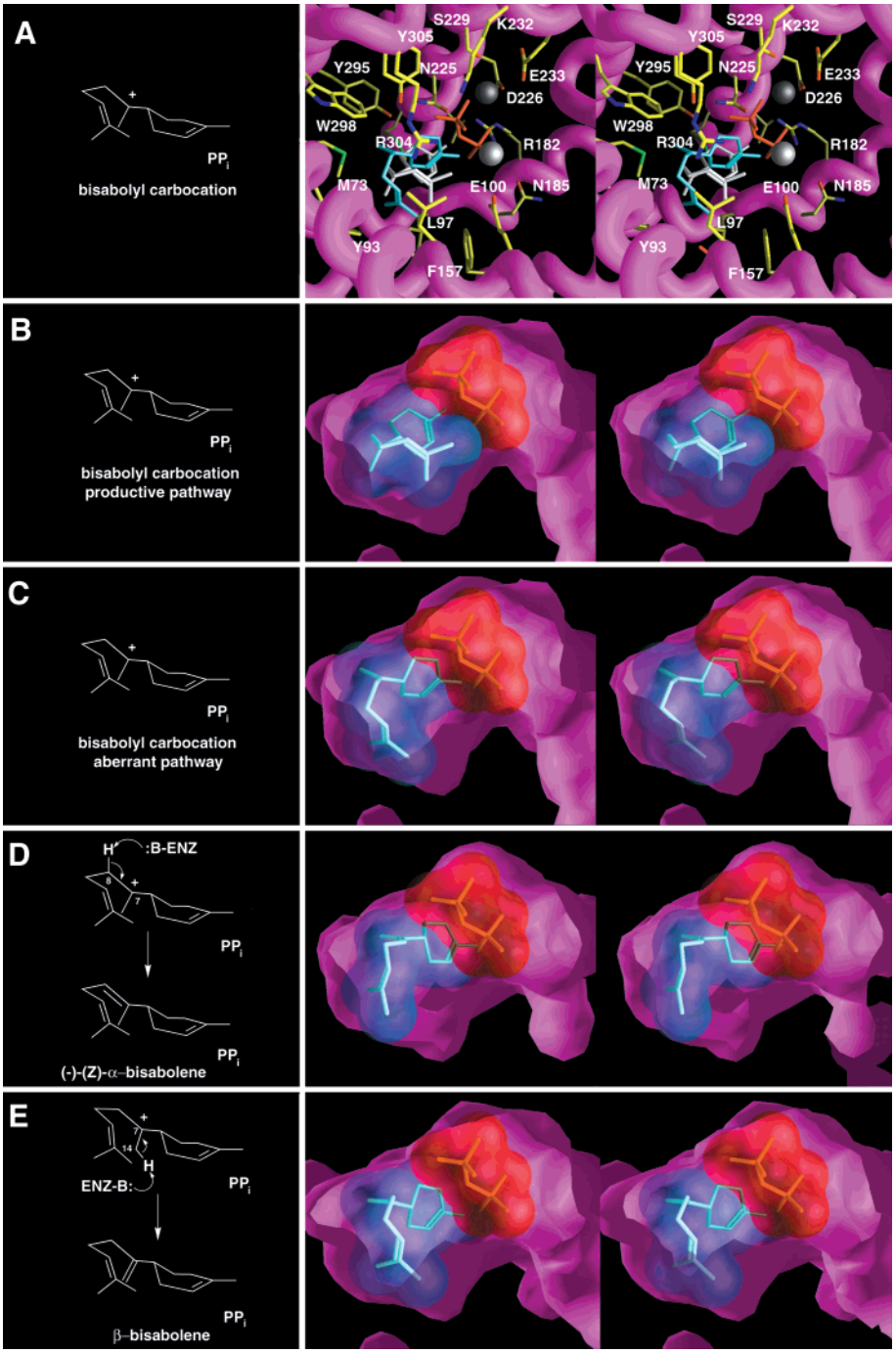

FIGURE 6: Alternate product formation from the bisabolyl carbocation intermediate. The model of the bisabolyl carbocation has two conformations (A). The first (white) is similar to the wild-type model. The second (cyan) is allowed by the greater active site volume of D100E trichodiene synthase. Both productive (B) and aberrant (C) conformations fit well into the active site cavity as evidenced by the molecular surface renderings of the protein (magenta), bisabolyl carbocation (cyan), and pyrophosphate (red). Deprotonation of C8, possibly by the side chain of Y305, results in the formation of α-bisabolene (D). Deprotonation of C14, possibly by the side chain of Y295, results in the formation of *β*-bisabolene (E). This figure was prepared with GRASP (*24*).

ates along the normal reaction pathway, and one results from a ring expansion migration reaction. As previously mentioned, the active site is 12% larger in the D100E mutant than in the wild-type enzyme, increasing from 324 to 364 Å^3, respectively. Notably, as the substrate undergoes cyclization, its hydrocarbon volume decreases: the hydrocarbon portion of farnesyl diphosphate is approximately 244 Å^3 whereas the volume of trichodiene is 230 Å^3. In other words, in the substrate → intermediates → products succession, progressively smaller molecules are contained in a larger active site cavity. Decreasing volume is thus potentially accompanied by increased susceptibility to nonproductive reactions. We now rationalize the formation of each aberrant product in view of the crystal structure of D100E trichodiene synthase.

The acyclic sesquiterpene *β*-farnesene results from deprotonation at C15 of either farnesyl diphosphate, (3*R*)-nerolidyl diphosphate, or the corresponding allylic cation. In the model of the D100E trichodiene synthase−nerolidyl diphosphate complex (Figure 5A,B), the C15 methyl group is close to the substrate diphosphate group, suggesting that this species could potentially deprotonate C15. This abortive pathway

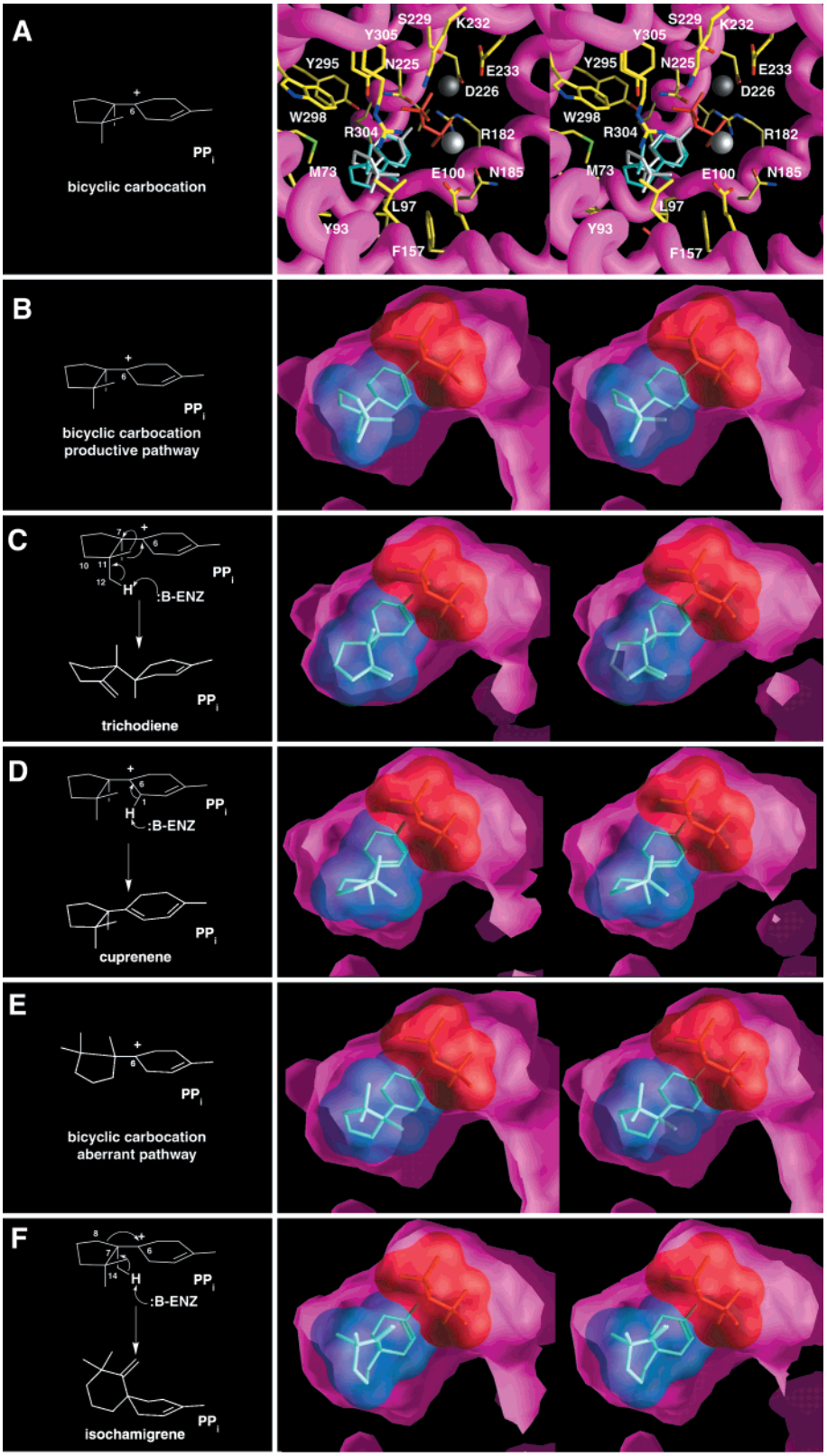

FIGURE 7: Alternate product formation from the C6 carbocation intermediate. The model of the C6 carbocation shows two potential conformations in the active site: one consistent with the formation of trichodiene and cuprenene (white) and the other consistent with the formation of isochamigrene (cyan). Increased conformational freedom results from increased active site volume in D100E trichodiene synthase (A). The productive conformation fits well into the active site as indicated by the molecular surface rendering of the protein (magenta), bicyclic carbocation (cyan), and diphosphate (red) (B). Two methyl migrations and deprotonation of C12 by either pyrophosphate or the side chain of E100 in this conformation lead to trichodiene production (C). Deprotonation of C1, possibly by pyrophosphate, in this intermediate leads to the production of cuprenene (D). The aberrant pathway conformation for the bicyclic carbocation is also accommodated by the larger active site of the mutant (E). A ring expansion and deprotonation of C14 by pyrophosphate leads to the formation of isochamigrene (F). This figure was prepared with GRASP (*24*).

yielding β-farnesene prevents the formation of a cyclic terpene product (Figure 5C). On the basis of the observed product distribution, the productive pathway of cyclization to the bisabolyl carbocation partitions with this nonproductive pathway with a ratio of 88:11 (*11*). Thus, the D100E substitution introduces a branch point with an energetic separation of 1.25 kcal mol^{-1} that nevertheless favors the productive cyclization pathway over the nonproductive quenching pathway.

All five cyclic terpene products (including trichodiene) require the formation of the bisabolyl carbocation intermediate (Figure 6A−C). The D100E substitution sustains the main ring closure reaction to yield the bicyclic carbocation intermediate, but this pathway partitions with two other deprotonation reactions that prematurely quench the bisabolyl carbocation to yield (−)-(*Z*)-α-bisabolene (11% relative yield) and β-bisabolene (11% relative yield). Possible rotation of the bisabolyl carbocation in the active site accommodated by the larger active site cavity positions C8 for deprotonation by the side chain of Y305 (Figure 6D) and positions C14 for deprotonation by the side chain of Y295 (Figure 6E). In the wild-type enzyme, the substrate appears to be more restricted and cannot rotate in this fashion. On the basis of the observed product distributions, bicyclic carbocation formation partitions with α-bisabolene and β-bisabolene formation with a ratio of 66:11:11; i.e., an energetic difference of 0.66 kcal mol^{-1} separates the productive pathway of bicyclic carbocation formation from the two premature quenching pathways introduced by the D100E substitution. Despite the introduction of this branch point in the cyclization cascade, the productive cyclization pathway remains favored but less so than in the previous step.

From the bicyclic carbocation intermediate (Figure 7A), two nonproductive pathways are introduced in the D100E mutant. A 1,4 hydride transfer followed by deprotonation at C1 leads to the formation of cuprenene (7% relative yield) (Figure 7D). In the models, C1 is located close to pyrophosphate, which may play the role of the catalytic base to generate cuprenene. The shift of pyrophosphate from its position in the wild-type enzyme may explain why this deprotonation pathway only occurs in the mutant. Alternatively, after the 1,4 hydride transfer, the substrate can rotate about the C6−C7 bond such that the σ bond of C7−C8 overlaps with the empty π orbital of the C6 carbocation (Figure 7E,F). Expansion of the five-membered ring to a six-membered ring forms the new C6−C8 bond. The resulting carbocation at C7 is quenched by deprotonation from C14 to form isochamigrene (14% relative yield). Notably, rotation about the C6−C7 bond is sterically hindered in the wild-type model but appears to be allowed in the D100E mutant due to the 12% greater volume of the active site cavity. The occurrence of C6−C7 bond rotation also suggests that the C6 carbocation is fairly long lived. This rotation potentially positions C14 for deprotonation by the paired diphosphate ion. On the basis of the observed product ratios after formation of the five-membered ring intermediate, the productive pathway of trichodiene formation (Figure 7B,C) remains favored by 0.46 kcal mol^{-1} over the aberrant cyclization pathways.

As the cyclization cascade proceeds, the volume of the hydrocarbon skeleton of the various intermediates decreases at each branch point from farnesyl diphosphate (244 Å^3) to the bisabolyl carbocation (240 Å^3) to the product trichodiene (230 Å^3). As the substrate volume decreases, the energetic gaps separating the trichodiene biosynthetic pathway from aberrant pathways also decrease, from 1.25 kcal mol^{-1} for the pathway leading to the acyclic sesquiterpene β-farnesene to 0.46 kcal mol^{-1} for the pathway leading to isochamigrene and cuprenene. Thus, the larger active site of the D100E mutant becomes increasingly less effective as a template for conformational control of increasingly smaller reactants as the cyclization proceeds.

CONCLUSIONS

The crystal structure of D100E trichodiene synthase is the first of a site-specific mutant of a terpenoid cyclase in which an amino acid substitution has been made in the aspartate-rich motif. Comparison of wild-type and D100E trichodiene synthases complexed with pyrophosphate reveals the structural basis of product diversity in the mutant: a larger active site cavity that is less effective as a template for the exclusive production of trichodiene. Increased spatial and conformational freedom of the substrate and reactive intermediates leads to increased nonproductive side reactions that yield aberrant products.

Notably, the volume of the hydrocarbon portion of substrate farnesyl diphosphate is 244 Å^3, and the active site volume of the wild-type enzyme−pyrophosphate complex is 324 Å^3. It follows that the substrate binds in the active site cavity with a packing density of 75%. This value is comparable to that of 74% for close-packed identical spheres, it is within the range of 70−78% measured for crystals of small organic molecules, and it is identical to the average packing density of the interior of a folded protein (*25*). Thus, the active site template in a high-fidelity (i.e., single-product) terpenoid cyclase has evolved to optimize the packing density of the substrate and reaction intermediates in the enzyme active site. In the D100E mutant (active site volume = 364 Å^3), enzyme−substrate packing density decreases to 67%, and this is sufficient to open up alternate reaction pathways with relatively small energetic barriers. Moreover, these energetic barriers decrease with decreasing packing density of successively formed reaction intermediates. Simply put, the lower the packing density of the terpenoid substrate or carbocation intermediate, the greater the chances of aberrant product formation. Possibly, aberrant product formation in other site-specific mutants of trichodiene synthase, or even evolutionary mechanisms that broaden or redirect the product diversity of terpenoid cyclases, can be explained from the basis of relaxed packing density in enzyme−substrate and/or enzyme−intermediate complexes.

ACKNOWLEDGMENT

We thank the Advanced Photon Source Structural Biology Center for beamline access.

REFERENCES

1. Cane, D. E. (1985) *Acc. Chem. Res. 18*, 220−226.
2. Croteau, R., and Cane, D. E. (1985) *Methods in Enzymology. Steroids and Isoprenoids (Part A)* Vol. 110, pp 383−405, Academic Press, New York.
3. Cane, D. E. (1990) *Chem. Rev. 90*, 1089−1103.
4. Wendt, K. U., and Schulz, G. E. (1998) *Structure 6*, 127−133.

5. Lesburg, C. A., Caruthers, J. M., Paschall, C. M., and Christianson, D. W. (1998) *Curr. Opin. Struct. Biol. 8*, 695−703.
6. Lesburg, C. A., Zhai, G., Cane, D. E., and Christianson, D. W. (1997) *Science 277*, 1820−1824.
7. Starks, C. M., Back, K., Chappell, J., and Noel, J. P. (1997) *Science 277*, 1815−1820.
8. Caruthers, J. M., Kang, I., Rynkiewicz, M. J., Cane, D. E., and Christianson, D. W. (2000) *J. Biol. Chem. 275*, 25533−25539.
9. Rynkiewicz, M. J., Cane, D. E., and Christianson, D. W. (2001) *Proc. Natl. Acad. Sci. U.S.A. 98*, 13543−13548.
10. Tarshis, L. C., Proteau, P. J., Kellogg, B. A., Sacchettini, J. C., and Poulter, C. D. (1996) *Proc. Natl. Acad. Sci. U.S.A. 93*, 15018−15023.
11. Cane, D. E., Xue, Q., and Fitzsimons, B. C. (1996) *Biochemistry 35*, 12369−12376.
12. Cane, D. E., Xue, Q., Van Epp, J. E., and Tsantrizos, Y. S. (1996) *J. Am. Chem. Soc. 118*, 8499−8500.
13. Cane, D. E., Wu, Z., Oliver, J. S., and Hohn, T. M. (1993) *Arch. Biochem. Biophys. 300*, 416−422.
14. Otwinowski, Z., and Minor, W. (1997) *Methods in Enzymology. Macromolecular Crystallography (Part A)* Vol. 276, pp 307−326, Academic Press, San Diego.
15. Brünger, A. T., Adams, P. D., Clore, G. M., DeLano, W. L., Gros, P., Grosse-Kunstleve, R. W., Jiang, J.-S., Kuszewski, J., Nilges, M., Pannu, N. S., Read, R. J., Rice, L. M., Simonson, T., and Warren, G. L. (1998) *Acta Crystallogr. D54*, 905−921.
16. Jones, T. A., Zou, J. Y., Cowan, S. W., and Kjeldgaard, M. (1991) *Acta Crystallogr. A47*, 110−119.
17. Mohamadi, F., Richards, N. G. J., Guida, W. C., Liskamp, R., Lipton, M., Caufield, C., Chang, G., Hendrickson, T., and Still, W. C. (1990) *J. Comput. Chem. 11*, 440−467.
18. Cane, D. E., and Yang, G. (1994) *J. Org. Chem. 59*, 5794−5798.
19. Cane, D. E., Yang, G., Xue, Q., and Shim, J. H. (1995) *Biochemistry 34*, 2471−2479.
20. Cane, D. E., Chiu, H.-T., Liang, P.-H., and Anderson, K. S. (1997) *Biochemistry 36*, 8332−8339.
21. Kleywegt, G. J., and Jones, T. A. (1993) *CCP4/ESF-EACBM Newsl. Protein Crystallogr. 29*, 26−28.
22. Kleywegt, G. J., and Jones, T. A. (1994) *Acta Crystallogr. D50*, 178−185.
23. Kleywegt, G. J., Zou, J. Y., Kjeldgaard, M., and Jones, T. A. (2001) in *International Tables for Crystallography* (Rossmann, M. G., and Arnold, E., Eds.) Vol. F, pp 353−356, 366−367, Kluwer Academic Publishers, Dordrecht, The Netherlands.
24. Nicholls, A., Sharp, K. A., and Honig, B. (1991) *Proteins 11*, 281−296.
25. Creighton, T. E. (1993) in *Proteins: Structure and Molecular Properties*, 2nd ed., p 229, W. H. Freeman and Co., New York.

BI011960G